ISBN: 978-3-95450-261-5 ISSN: 2673-7000 doi: 10.18429/JACoW-NAPAC2025-MOP052

DESIGN OF A BPM PICK-UP FOR THE EIC ELECTRON STORAGE RING*

M. Sangroula†, J. Bellon, A. Blednykh, D. Gassner, C. Hetzel, C. Liu, I. Pinayev, M. Wendt
Brookhaven National Laboratory, Upton, NY, USA

Abstract

A new beam position monitor (BPM) pick-up, compatible to operate reliably with the high current electron beams foreseen in the 5 - 18 GeV Electron Storage Ring (ESR) of the Electron-Ion Collider (EIC) project, is presented. We discuss a few design options for this button-style BPM pick-up with a focus on output signal levels, position characteristic, and wakefield effects. Regarding the octagonal cross-section geometry of the ESR vacuum chamber, the BPM pick-up analysis relies on numerical methods, here performed using the CST Studio software.

INTRODUCTION

The Electron-Ion Collider (EIC) [1–4], presently in the design phase, will enable collisions between polarized electron and hadron beams at center-of-mass energies ranging from 30 to 140 GeV/nucleon. The collider consists of two main rings, an Electron Storage Ring (ESR) and a Hadron Storage Ring (HSR), both reside in RHIC tunnel having a 3.8 km circumference. The vacuum chamber of the ESR is made of copper and has an octagonal cross-section shape with 80 mm (horizontal) × 36 mm (vertical) aperture. While operating with the highest beam current, up to 2.5 A, comprised of short electron bunches (σ = 7 mm), refer to Table 1, in the ESR poses several design challenges for the 220 beam position monitors (BPMs). These challenges include elevated beam-induced resistive wall (RW) heating, achieving acceptable beam-coupling impedance to ensure beam stability, and providing sufficient position measurement resolution, accuracy and reproducibility, all required to achieve high luminosity and preserve polarization.

Table 1: ESR Beam Parameters for the Highest RW Heating

Parameters	Value	Unit
Bunch length (σ_{rms})	7	mm
Average beam current	2.5	A
Charge per bunch (Q_b)	27.6	nC
Number of bunches (N_b)	1160	
Beam energy	5 & 10	GeV

THE ESR BUTTON BPM PICK-UP

Button BPMs are the most popular and cost-effective type of pick-up to monitor the beam centroids of short electron bunches in electron storage rings. We will use button BPMs throughout all the EIC accelerator complex, including the EIC Electron Storage Ring (ESR). Figure 1 (a) illustrates the geometry of the ESR button BPM pick-up mounted to the octagonal shaped copper vacuum chamber. It consists of two flanges - top and bottom - each housing two molybdenum button electrodes of 7 mm diameter, are housed as pairs, separated by 22 mm in two 304L stainless-steel flanges mounted on top and bottom of the vacuum pipe (cooling channels not shown). While we used the detailed geometry, Fig. 1 (a), for the numerical analysis of the BPM including the losses in the metals, we used a simplified model, Fig. 1 (b), to find the relevant details to analyze the position characteristic and the geometric wakefield effects. For the simulation setup, we used *normal* (vacuum: $\varepsilon_r = 1,\ \mu_r = 1$) background in the former case, and *perfect electric conductor* (PEC) in the later lossless analysis.

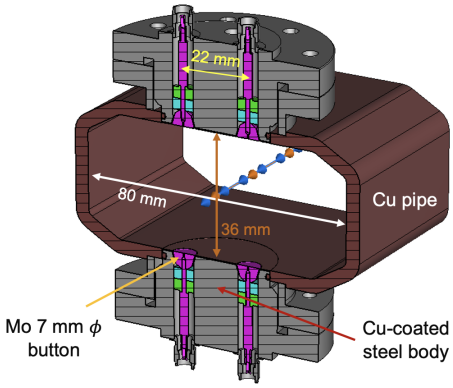

(a) ESR BPM geometry with materials indicated

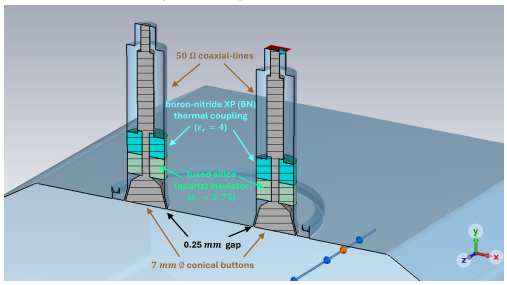

(b) Simplified model for the loss free analysis

Figure 1: Cross-section view of the ESR BPM pick-up assembly.

An alternative button electrode with simple cylindrical button shape instead of conical, and with the same button diameter, and other dimensions, see Fig. 2, was used for a comparative lossless study. Due to the octagonal cross-section of the vacuum chamber, analytical methods are not feasible for this button BPM design. Therefore, numerical

* Work supported by Brookhaven Science Associates, LLC under Contract No. DE-SC0012704 with the U.S. Department of Energy.
† msangroul@bnl.gov

ISBN: 978-3-95450-261-5 ISSN: 2673-7000 doi: 10.18429/JACoW-NAPAC2025-MOP052

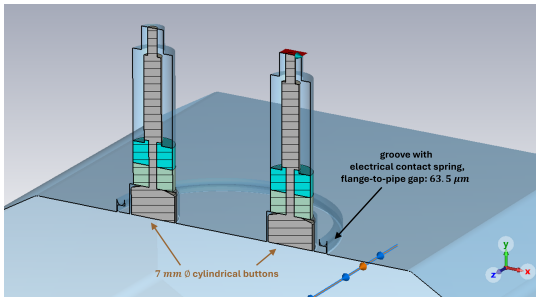

Figure 2: Cylindrical button BPM for loss free analysis.

simulations were carried out using the CST Studio suite [5], employing both electrostatic and wakefield solvers.

SIGNAL AND BEAM POSITION CHARACTERISTIC

The output signal behavior of a button BPM electrode depends on the beam induced image charges on the vacuum chamber walls. The voltage on the electrode follows:

$$V_{elec}(x,y,f) = k(x,y)Z_{elec}(f)I_b(f) \tag{1}$$
$$\Rightarrow\ v_{elec}(x,y,t) = k(x,y)\int_{-\infty}^{+\infty} df Z_{elec}(f)I_b(f)e^{i2\pi ft}$$

where $k(x,y)$ is the *coupling sensitivity* of the electrode, which is frequency-independent function having its value $0 < k < 1$ depending upon the transverse (x,y) beam position, $Z_{elec}(f)$ is the *transfer impedance* of the electrode, usually of 50 Ω. $I_b(f)$ is the frequency-domain equivalent of the longitudinal particle distribution function of the *Gaussian* bunch:

$$i_b(s) = \frac{Q_b}{\sigma\sqrt{2\pi}}e^{-\frac{1}{2}\left(\frac{s}{\sigma}\right)^2} \equiv i_b(t) = \frac{Q_b}{\sigma_t\sqrt{2\pi}}e^{-\frac{1}{2}\left(\frac{t}{\sigma_t}\right)^2} \tag{2}$$

Figure 3 shows the output voltage signal of the button electrode, Fig. 3a in time- and Fig. 3b frequency-domain, for an on-axis beam of $\sigma = 7$ mm, $Q_b = 1$ nC, where $k(x = y = 0) \approxeq 0.05$. Figure 3 shows that the output signal of the conical button is ∼ 30 % larger than that of the cylindrical button although their output signal waveforms are similar. While the frequency spectrum of the button electrode signal in Fig. 3 due to a 7 mm bunch length extends well above 10 GHz, here we limit the graph shown as modulus on a

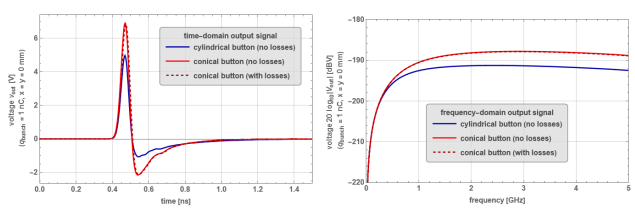

(a) Time-domain (b) Frequency-domain

Figure 3: ESR button electrode output signal.

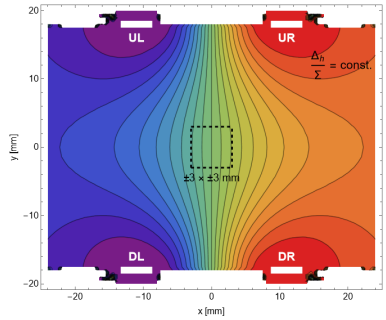

Figure 4: Normalized horizontal position measurement gradients for the ESR BPM.

logarithmic *dBV*-scale to a range $DC - 5$ GHz, which is more relevant for the BPM read-out electronics design.

To monitor transverse beam position, which is independent of bunch-intensity, the output signals due to all four button electrodes need to be normalized. For this, we applied the popular Δ/Σ method:

$$Hor.\ pos. \propto \frac{\Delta_h}{\Sigma} = \frac{(v_{UR}+v_{DR})-(v_{UL}-v_{DL})}{v_{UR}+v_{DR}+v_{UL}+v_{DL}}$$
$$Vert.\ pos. \propto \frac{\Delta_v}{\Sigma} = \frac{(v_{UR}+v_{UL})-(v_{DR}-v_{DL})}{v_{UR}+v_{DR}+v_{UL}+v_{DL}} \tag{3}$$

with v_{RS} being the four electrode signal voltages, each following v_{elec} of Eq. (1), acquired by a set of analog-to-digital converters (ADC). As the position behacior of each BPM electrode $k(x,y)$ is frequency-independent, Eq. (3) can be analyzed by solving the *Laplace* equation; $\nabla^2\Phi_{elec}(\mathbf{r}) = 0$, as simple electrostatic problem for one of the four button electrodes and by means of applying the *Green's reciprocity theorem*.

Figure 4 illustrates the normalized position behavior as parametric plot $\Delta_h/\Sigma = const.$ as an example for the horizontal plane. This demonstrates the non-linear behavior of the BPM, also indicated is the nominal $x, y = \pm 3$ mm operating range.

Fortunately, the position nonlinearities can be corrected. To correct this, we applied a set of 2D polynomial fit-functions

$$\begin{cases} x^{2D}_{BPM} = \sum_{i,j=0}^{p,q}(c_{ij}x^i_{raw}y^j_{raw}) = Q_{pq}(x_{raw},y_{raw}) \approx x \\ y^{2D}_{BPM} = \sum_{i,j=0}^{p,q}(c_{ij}y^i_{raw}x^j_{raw}) = Q_{pq}(y_{raw},x_{raw}) \approx y \end{cases} \tag{4}$$

of 5$^{\text{th}}$-order ($Q_{pq} = Q_{54}$) to the inverted horizontal and vertical position characteristic:

$$\begin{cases} x = f^{-1}(x_{raw},y_{raw}) \\ y = g^{-1}(y_{raw},x_{raw}) \end{cases} \tag{5}$$

where $x_{raw} = \Delta_h/\Sigma$, $y_{raw} = \Delta_v/\Sigma$ are the raw measured, normalized beam positions, Eq. (3).

The corrected non-linear region for the beam for the ESR BPM is shown in Fig. 5a, and the absolute error is shown in Fig. 5b.

ISBN: 978-3-95450-261-5 ISSN: 2673-7000 doi: 10.18429/JACoW-NAPAC2025-MOP052

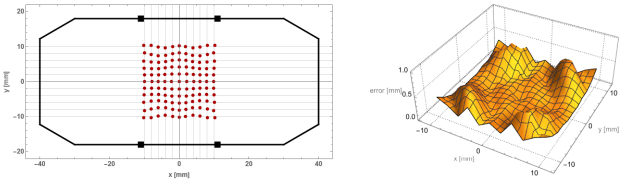

(a) Beam position after correction. (b) Absolute error

Figure 5: Correction of the position nonlinearities shown on a 10×10 mm grid with 2 mm steps.

WAKEFIELD AND POWER LOSS ANALYSIS

The ESR beam parameters producing the highest resistive wall (RW) heating, as the worst-case scenario, are listed in Table 1. We performed wakefield and impedance analysis for the ESR BPM with these beam parameters. Figure 6 shows the longitudinal wake potential comparison for both conical and cylindrical button types as shown in Figs. 1 and 2, obtained from CST wakefield solver, where the blue curve represents the longitudinal wake potential for the cylindrical button (loss free), the solid red curve represents conical button (loss free), and the dash red curve represents conical button with losses. From this wake potential comparison, Fig. 6, it seems surprising that the loss factor (k_{loss}) for the cylindrical button is lower than for the conical one. The difference in k_{loss} value for the conical button BPM (with and without losses) is related to the resistivity of materials.

The Fourier transform of the wakefield is called impedance. Figure 7 shows the real and imaginary parts of the longitudinal impedance along with the bunch spectrum (green curve). The cylindrical button design (dark blue curve) shows resonances at slightly lower frequency than that of conical button geometry (red curve) however, the manufacturing cost associated with the conical button is higher than that of cylindrical design.

In addition to wakefield and impedance analysis, we evaluated the beam-induced RW losses for the ESR BPM with conical button as shown in Fig. 1(a), using the beam parameters listed in Table 1. The total power dissipation based on the loss factor (k_{loss}), where $\Delta E_b = Q_b^2 k_{loss}$, is given by

$$P_{loss\_field} = \frac{\Delta E_b}{t_{rev}} N_b \quad \approxeq 30.79\,\text{W}. \qquad (6)$$

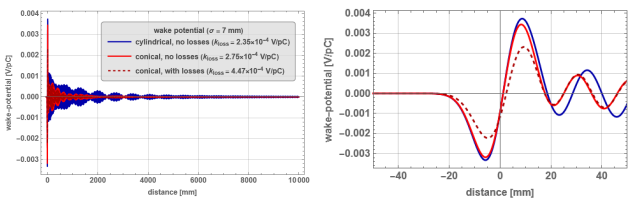

(a) Long range wake. (b) Short range wake.

Figure 6: Longitudinal wake potential of the ESR BPM.

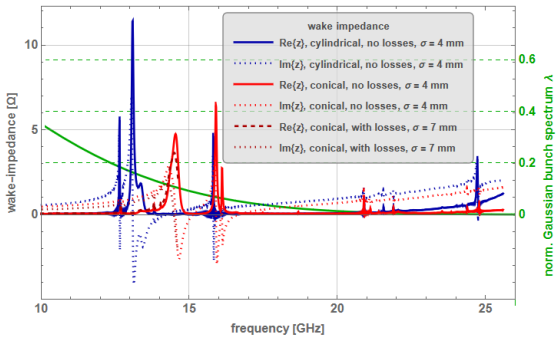

Figure 7: Real and imaginary parts of the longitudinal wake impedance for the ESR BPM pick-up.

Table 2: RW Losses in the Metals for the BPM Pick-up

Components	Materials	Value
2-Button body inner surface	Cu-coated st.	2.72 W
2-Button body	SS 304L	3.27 W
4-BPM buttons & stems	Molybdenum	1.16 W
Beam pipe (100 mm long)	Copper	7.62 W

For the calculation of Eq. (6), we used $t_{rev} \approxeq 12.7885\,\mu$s and included the signal output power in the four ports. While subtracting the power loss via four waveguide ports, we can evaluate the RW losses in different metals, which are listed in Table 2. The electrical conductivities used in this analysis, at room temperature, were 5.8×10^7 S/m for annealed copper, 1.3888×10^7 S/m for stainless steel 304L, and 1.82×10^7 S/m for molybdenum.

The preliminary thermal analysis for the ESR BPM with elliptical vacuum chamber can be found in [6], which showed the button temperature within the acceptable limit. We plan to update this thermal analysis with the recent octagonal shaped vacuum chamber after selecting the design. The papers on the beam induced heating and thermal analysis for the various EIC vacuum chamber components can be found in References [7–11].

SUMMARY

In this paper, we discussed the design of the ESR BPM pick-up to address challenges associated with providing reliable beam position measurements, acceptable geometric impedance related to the button geometry, and high beam-induced RW losses due to short & high-charge electron bunches. CST simulation shows that the conical button geometry offers the better impedance performance compared to the cylindrical button. However, the cost and fabrication complexity of the conical button will likely be higher. As the design matures, a button geometry decision will be made to ensure fabrication feasibility, reliability, cost effectiveness, and that the performance requirements are met.

ISBN: 978-3-95450-261-5 ISSN: 2673-7000 doi: 10.18429/JACoW-NAPAC2025-MOP052

REFERENCES

[1] Electron-Ion Collider. https://www.bnl.gov/eic/

[2] F. Willeke and J. Beebe-Wang, "Electron Ion Collider Conceptual Design Report", 2021. doi:10.2172/1765663

[3] C. Montag *et al.*, "Design status of the Electron-Ion Collider", in *Proc. IPAC'23*, Venice, Italy, pp. 136–139, 2023. doi:10.18429/JACoW-IPAC2023-MOPA049

[4] C. Montag *et al.*, "The EIC accelerator: design highlights and project status", in *Proc. IPAC'24*, Nashville, TN, USA, pp. 214–217, 2024. doi:10.18429/JACoW-IPAC2024-MOPC67

[5] CST Studio Suite Electromagnetic Simulation Solvers. https://www.3ds.com/products-services/simulia/products/cst-studio-suite/solvers/

[6] M. P. Sangroula *et al.*, "Localized Beam Induced Heating Analysis of the EIC Vacuum Chamber Components", in *Proc. NAPAC'22*, Albuquerque, NM, USA, pp. 833–836, 2022. doi:10.18429/JACoW-NAPAC2022-WEPA85

[7] M. Sangroula *et al.*, "Beam Induced Heating Analysis Update For The EIC Vacuum Chamber Components", Brookhaven National Laboratory (BNL), Upton, NY , USA, Tech. Rep., 2023.

[8] F. Micolon, D. Gassner, C. Hetzel, I. Pinayev, M. Sangroula, and S. Verdu-Andres, "Thermal Simulation of the HSR arc BPM Module for EIC", Brookhaven National Laboratory (BNL), Upton, NY , USA, Tech. Rep., 2023.

[9] S. Verdu-Andres and M. Sangroula, "Beam-induced Heat Deposition in the EIC HSR Screen", Brookhaven National Laboratory (BNL), Upton, NY , USA, Tech. Rep., 2023.

[10] M. Sangroula *et al.*, "Resistive wall heating and thermal analysis of the EIC HSR beam screen", in *Proc. IPAC'24*, Nashville, TN, USA, pp. 759–762, 2024. doi:10.18429/JACoW-IPAC2024-MOPS22

[11] M. Sangroula *et al.*, "Update on the beam-induced heating and thermal analysis for the EIC vacuum chamber components", in *Proc. IPAC'24*, Nashville, TN, USA, pp. 755–758, 2024. doi:10.18429/JACoW-IPAC2024-MOPS21